

6-1-2007

Remotely adjustable check-valves with an electrochemical release mechanism for implantable biomedical microsystems

Tingrui Pan

Department of Biomedical Engineering, UC Davis

Antonio Baldi

Centro Nacional de Microelectrónica

Babak Ziaie

Birck Nanotechnology Center, Purdue University, bziaie@purdue.edu

Follow this and additional works at: <http://docs.lib.purdue.edu/nanodocs>

Pan, Tingrui; Baldi, Antonio; and Ziaie, Babak, "Remotely adjustable check-valves with an electrochemical release mechanism for implantable biomedical microsystems" (2007). *Other Nanotechnology Publications*. Paper 55.
<http://docs.lib.purdue.edu/nanodocs/55>

This document has been made available through Purdue e-Pubs, a service of the Purdue University Libraries. Please contact epubs@purdue.edu for additional information.

Remotely adjustable check-valves with an electrochemical release mechanism for implantable biomedical microsystems

Tingrui Pan · Antonio Baldi · Babak Ziaie

Published online: 25 January 2007
© Springer Science + Business Media, LLC 2007

Abstract In this paper, we present two remotely adjustable check-valves with an electrochemical release mechanism for implantable biomedical microsystems. These valves allow one to vary the opening pressure set-point and flow resistance over a period of time. The first design consists of a micromachined check-valve array using a SU-8 polymer structural layer deposited on the top of a gold sacrificial layer. The second design is based on a variable length cantilever beam structure with a gold sacrificial layer. The adjustable cantilever-beam structure is fabricated by gold thermo-compression bond of a thin silicon wafer over a glass substrate. In both designs, the evaporated gold can be electrochemically dissolved using a constant DC current via a telemetry link. In the first design the dissolution simply opens up individual outlets, while in the second design, gold anchors are sequentially dissolved hence increasing the effective length of the cantilever beam (reducing the opening pressure). A current density of 35 mA/cm² is used to dissolve the gold sacrificial layers. Both gravity and syringe-pump driven flow are used to characterize the valve performance. A multi-stage fluidic performance (e.g. flow resistance and opening pressure) is clearly demonstrated.

Keywords Microfluidic · Microvalve · Wireless implantable microsystem · Gold dissolution · Glaucoma

1 Introduction

Micromachined passive check-valves play an important role in a variety of implantable biomedical microsystems (e.g., drug delivery and therapeutic pressure relief devices) (Gretzinger et al., 1995; Wang et al., 1999; Low et al., 2000; Qing et al., 2001). In many applications, it is highly desirable to be able to vary the opening pressure set-point and flow resistance over a period of time (Pan et al., 2002, 2005). For example, valved glaucoma drainage devices (valved-GDDs) incorporate a passive check valve to reduce the intra-ocular pressure (IOP). Recent studies have shown that subsequent to the fibrous capsule formation around valved-GDDs after implantation, the IOP elevates significantly due to the additive resistance from the nanoporous structure of the fibrous capsule (Pan et al., 2003, 2005). Currently, there is no good solution to this problem other than performing another GDD implantation surgery, which leads to other complications such as bifocal problem (Shields, 1998). Therefore, the ability to remotely change the set-point after implantation provides the surgeon with the flexibility to regulate the IOP in the post-operation period. Other diseases, such as hydrocephalus, which require implantable pressure relief devices, could also benefit from this post-implant adjustment capability (Yoon et al., 2004). This paper reports on the fabrication and test of two designs of wireless, electrochemically-released, micromachined check-valves for implantable biomedical microsystems. Figure 1 shows a schematic of a wireless MEMS check-valve implanted on an eye, which could be remotely adjusted through an inductively powered telemetry link. Gold sacrificial layers or anchors are used to activate microma-

T. Pan
Department of Biomedical Engineering, UC Davis,
USA

A. Baldi
Centro Nacional de Microelectrónica (CNM-IMB), CSIC,
Spain

B. Ziaie (✉)
School of Electrical and Computer Engineering,
Purdue University, USA
e-mail: bziaie@purdue.edu

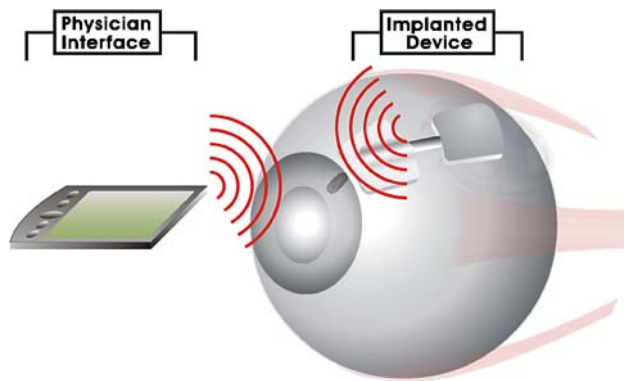


Fig. 1 Schematic of a wireless MEMS check-valve for an implantable glaucoma drainage device

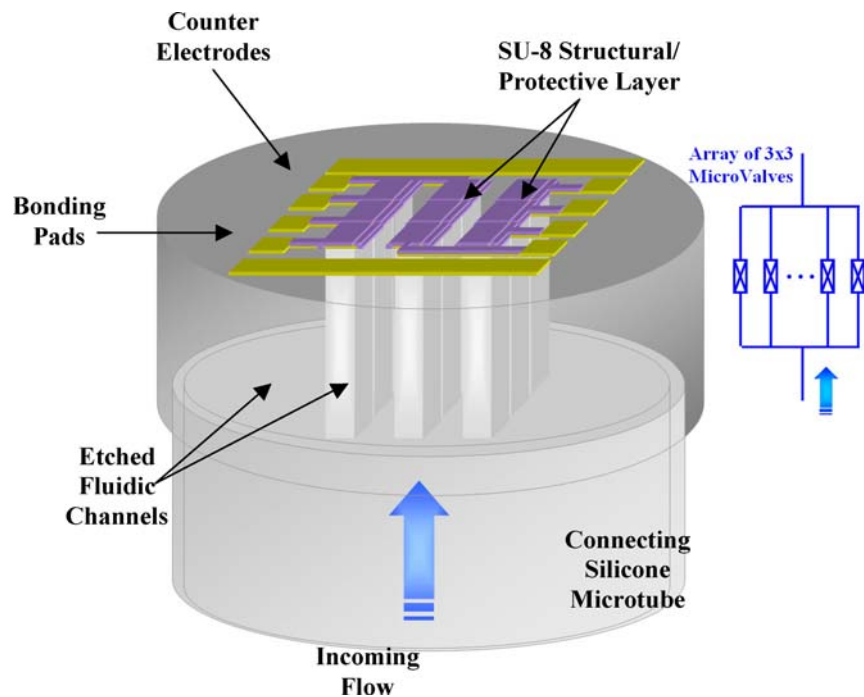
chined check-valves. This activation mechanism is based on the electrochemical dissolution of a thin gold membrane which occurs through the formation of water-soluble chloro-gold (III) complexes in the saline solution (Santini et al., 1999, 2000). The design, fabrication and test of two microvalves will be described in the following sections.

2 Design and fabrication of the SU-8 flap microvalve

2.1 Design

Figure 2 shows a 3D schematic representation of the device and its working principle. The device is composed by an array of micromachined check-valves working in parallel and connected to a silastic medical tubing. As can be seen, a SU-

Fig. 2 A 3D schematic of an array of micromachined check-valves connected to a silastic medical tubing with its working principle



8 layer is used as the microvalve structural material. SU-8 polymer is a negative photoresist, which is commonly used in high-aspect-ratio micromachining. Recent studies have indicated its suitability as a structural material with exceptional mechanical properties and good chemical stability. In addition, *in vivo* studies by Kotzar, et al. have shown that SU-8 is also biocompatible making it useful for implantable applications. Table 1 summarizes important thermomechanical properties of SU-8 (LaBianca and Delorme, 1995; Guerin et al., 1997; Lorenz et al., 1997, 1998).

The SU-8 layer is deposited on the top of a gold sacrificial layer which can be electrochemically etched through the application of a constant DC voltage (0.8–1.2 volts with respect to a saturated calomel reference electrode) or current (Santini et al., 1999, 2000). Gold dissolution occurs through the formation of water-soluble chloro-gold (III) complexes (Santini et al., 1999, 2000). This voltage/current can be easily generated via a telemetry link enabling one to remotely address and activate individual microvalves, which allows discretely decreasing the overall flow resistance of the device.

2.2 Fabrication

The microvalve array is fabricated using standard microelectromechanical system (MEMS) processes including chemical vapor deposition, lift-off, reactive ion etching and SU-8 photolithography. Figure 3 shows the fabrication process. It starts with silicon wafers with a $2\ \mu\text{m}$ low-pressure chemical vapor deposition (LPCVD) low-stress silicon nitride coating

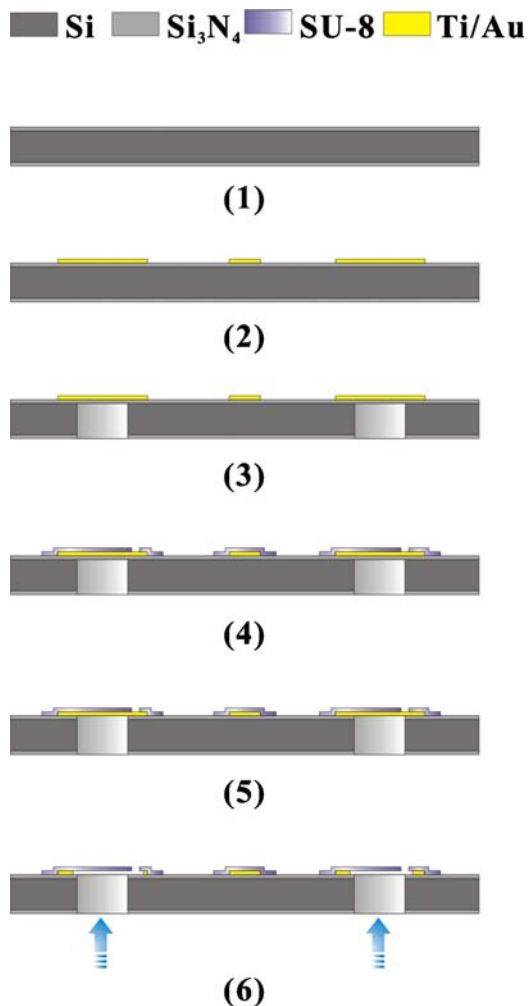


Fig. 3 Fabrication process for the SU8 check valve: (1) LPCVD of low stress silicon nitride; (2) e-beam evaporation and lift-off patterning of Ti/Au layer; (3) RIE and DRIE of silicon substrate from backside; (4) photolithography of SU-8 layer; (5) RIE of top nitride from backside; (6) electrochemical dissolution of gold membrane

on both sides. A chromium/gold (100 Å/3000 Å) layer is then deposited (e-beam evaporation) and patterned (lift-off). This layer acts both as the electrochemically actuated layer and as the electrical connection and bonding pads. The counter electrodes are patterned on this layer as well. Backside nitride and silicon are etched by reactive ion etching (RIE) and deep reactive ion etching (DRIE), respectively. Square-shaped orifices under each flap microvalve and packaging trenches (which will be discussed in detail in following section) are formed during these etch steps. SU-8 5 (MicroChem Corp., MA) is spun on top of the gold layer to serve as the structural and protective layer. The wafers are cleaned in isopropyl alcohol (IPA) prior to application of the SU-8 film. To achieve a better uniformity, the wafers are first accelerated to 3000 rpm over 5 sec followed by 30 sec of spinning at 3000 rpm. Subsequently, a two-stage soft bake is performed (1 min at 65°C and 5 min at 95°C). The wafers are then exposed to the UV source for 20 sec. A two-step post-exposure bake (PEB) is performed at 65°C and 95°C for 1 and 5 min, respectively. Optimum cross-link density is obtained through careful adjustments of the exposure and PEB process condition. SU-8 is then developed for 2 min followed by a rinse in IPA. An extra hard bake step at 150°C for 5 to 10 min is required for a structural SU-8 layer. Due to its large internal stress, numerous small cracks are usually formed in the SU-8 layer. The final hard bake eliminates the cracks and improves the mechanical robustness and chemical resistance. 3 × 3 and 4 × 4 arrays (total dimensions 2 × 2 and 4 × 4 mm²) each containing two different size valves (50 × 50 and 100 × 100 μm² flow channels) are fabricated and tested. Figure 4 shows a photograph of the 3 × 3 microvalve array bonded to a silastic medical tubing, along with a close-up micrograph of individual valves.

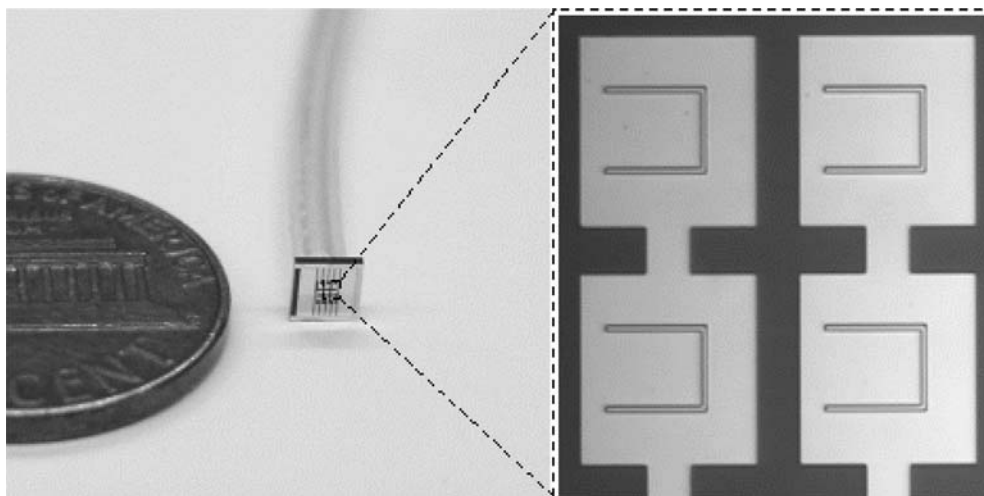
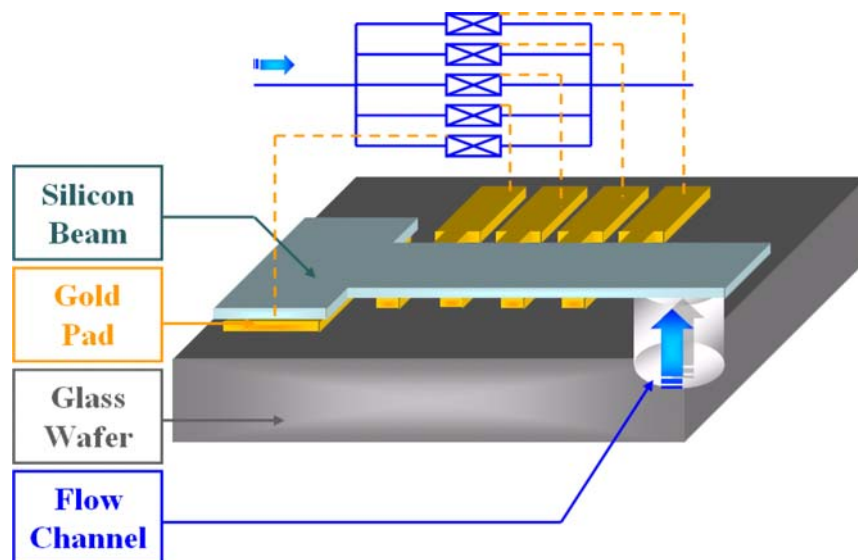


Fig. 4 A photograph of the 3 × 3 microvalve array bonded to a silastic medical tubing, along with a close-up micrograph of individual valves

Fig. 5 A perspective view of the microvalve along with its fluidic schematic



3 Design and fabrication of microvalve with a variable length cantilever-beam structure

3.1 Design

Using the same electrochemical dissolution mechanism as the SU-8 flap microvalve array, an alternative approach using a variable length cantilever-beam structure is also developed. Figure 5 shows a perspective view of the microvalve along with its fluidic schematic. It consists of a silicon cantilever beam bonded to a glass bottom plate containing an ultrasonically drilled inlet hole. The bonding is done using gold thermo-compression technique over selected areas defined by an array of gold anchor pads on the silicon substrate and thin gold strips on the glass substrate. An array of $10 \times 10 \mu\text{m}^2$ gold anchor pads with $10 \mu\text{m}$ separation is used in our design. On the glass substrate, the gold pattern is a continuous narrow strip of $50 \mu\text{m}$ wide connected to the outside pads. The gold anchors and strips define various lengths and hence opening pressures for the valve. The strips can be electrochemically removed in sequence, lowering the opening pressure accordingly.

3.2 Fabrication

Figure 6 shows the fabrication sequence. The silicon substrate fabrication process starts with a thermal oxidation step of a thin silicon substrate ($200 \mu\text{m}$ thick). A $0.5 \mu\text{m}$ silicon dioxide is grown to prevent silicon diffusion during thermo-compression bond (Tsau et al., 2002 #44); this also serves as an isolation layer during the electrochemical dissolution. The backside oxide layer is patterned for the final etching step. A Ti/Au ($10 \text{ nm}/1.0 \mu\text{m}$) bonding layer is then deposited by electron beam evaporation and patterned on the silicon wafer

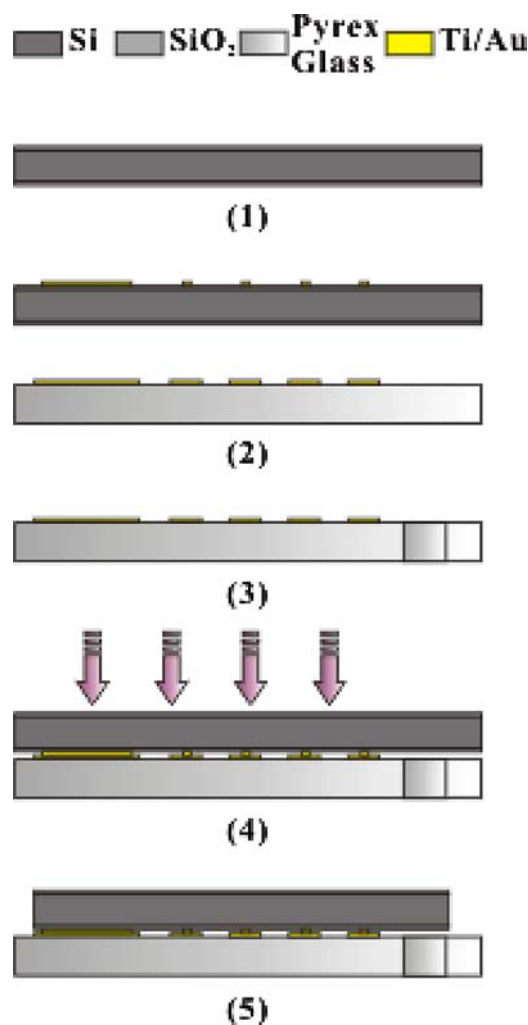


Fig. 6 Fabrication process includes: (1) thermal oxidation of silicon wafer; (2) e-beam evaporation and patterning of Ti/Au; (3) ultrasonic drilling of the flow channel; (4) thermo-compression bonding of Si-Glass; (5) DRIE Si from the backside followed by wafer dicing

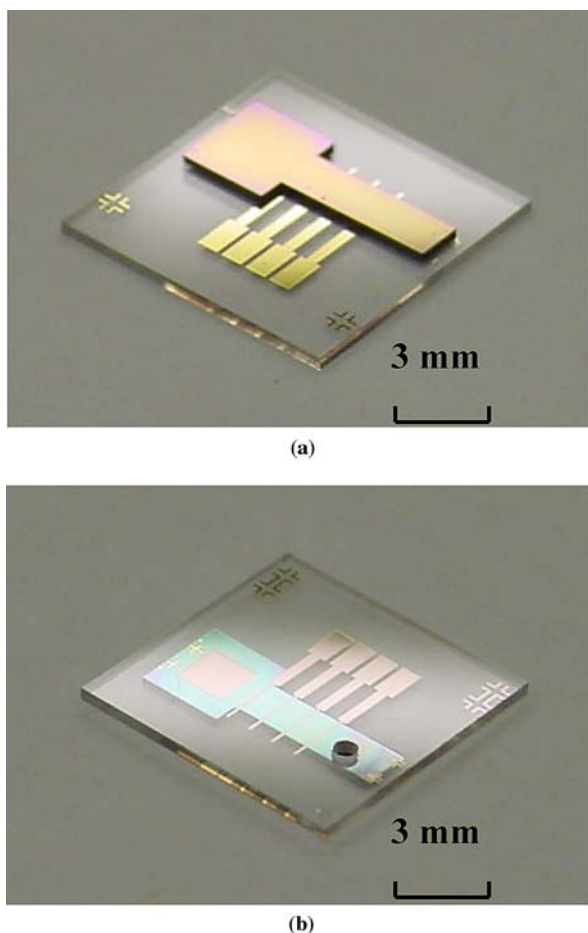


Fig. 7 Photographs of (a) the front view and (b) the backside view of the adjustable micromachined check-valve

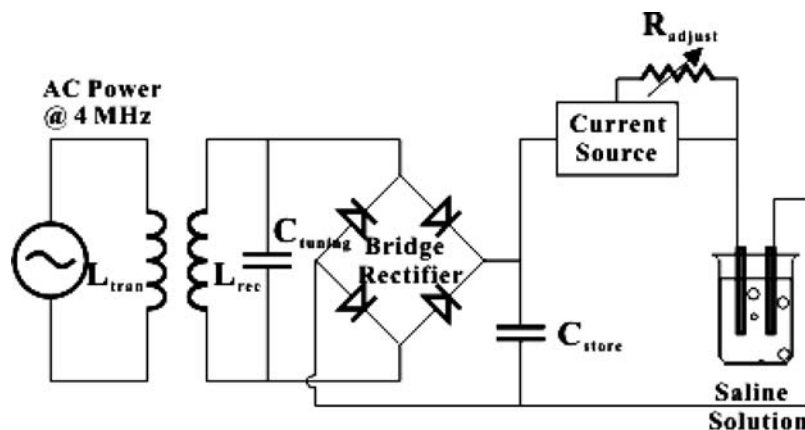
by lift-off process to create an array of gold bonding pads. The glass fabrication process starts with the deposition and patterning of the Ti/Au (10 nm/1.0 μm) bonding strips on a Pyrex 7740 glass substrate. A flow channel of 600 μm in diameter is then ultrasonically drilled on the glass substrate. The bonding surfaces of the two substrates are exposed to oxygen plasma for 5 min to completely remove organic re-

mains before wafer alignment. During the alignment process of two substrates, three spacers and three clamps on a bonder fixture are loaded consequentially to separate the wafers and hold them in position. The gold-to-gold thermo-compression is carried out in Karl Suss SB6 VAC bonder (Suss MicroTec, Germany) under atmospheric pressure. Following the withdrawal of the clamps, the temperature is ramped up and stabilized at 350°C for 30 min, 0.01 MPa pressure is applied over the wafer and spacers are withdrawn. Then a bonding pressure of 0.1 MPa is applied across the two substrates for 15 min (corresponding to 5 MPa of pressure on the gold anchor pads). Afterwards, the temperature is ramped down slowly (Tsau et al., 2002). To machine the silicon substrate into a cantilever shape, we use deep reactive ion etch (DRIE) from the backside of the silicon wafer. Finally, the devices are diced and separated into individual 8 × 8 mm² chips. The overall size is compatible with the currently implanted glaucoma drainage devices, e.g., Ahmed glaucoma valve (which is the most widely used implantable devices) is 13 mm wide, 16 mm long, and 2 mm thick. Figure 7 shows photographs of the front and the backside of the adjustable micromachined check-valve.

4 Results and discussion

The electrochemical activation of individual valves is carried out using a constant current source and an external gold counter electrode, as shown in Fig. 8. Constant-voltage schemes require a stable reference electrode in addition to the counter electrode, which makes this option less appealing for integrated and remotely operated systems. Both gravity and syringe-pump driven flow were used to characterize the valve performance (Porter et al., 1997). These can be easily achieved by using the setup shown in Fig. 9. The setup consists of a syringe pump (KDS Inc.) connected to a glass standpipe (1.1 mm ID) or a pressure sensor via a 3-way stop-cock. The third outlet is connected to the valve through a

Fig. 8 A schematic of the telemetry release setup



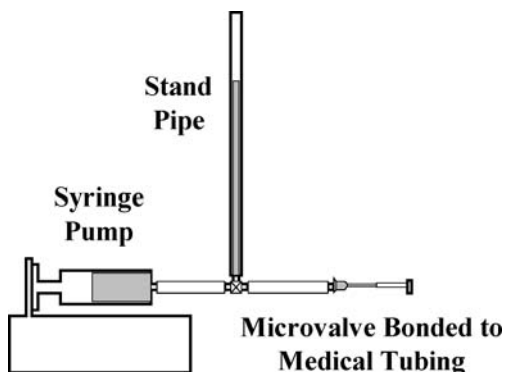


Fig. 9 Schematic of the *in vitro* microfluidic test setup for the microvalves

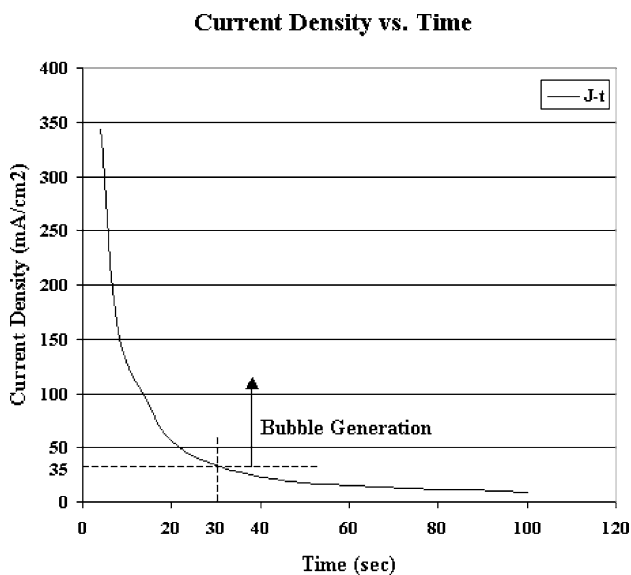


Fig. 10 Current density vs. release time for gold membranes (0.02 mm² of exposed area)

silastic tubing. All tests are carried out at the atmospheric pressure and room temperature.

In the gravity-driven flow tests, the branch connected to the syringe pump is closed and the valve is subjected to the

gravitational force of the fluid head, which forces the valve open and drains the fluid out until the gravitational head is reduced to the level at which the valve is closed. The flow rate through the device can be calculated as

$$Q = A \frac{dh}{dt} \tag{1}$$

where A is the cross-section area of the standpipe and h is the height of the fluid. The flow resistance, defined by the pressure drop P over the flow rate Q , can be obtained from

$$R = \frac{P}{Q} = \frac{P}{A \frac{dh}{dt}} \tag{2}$$

This configuration allows the flow resistance to be measured over a wide range of flow rates. In the syringe-pump driven tests, i.e., constant flow tests, the syringe pump provides a constant flow rate and pressure variation across the valve is monitored using the standpipe or a pressure sensor. This configuration also simulates the operation of pressure activated passive check valves encountered in actual physiological settings (e.g., constant aqueous humor inflow in the eye) (Brown and Brubaker, 1989).

4.1 SU-8 flap microvalve

Initially, we carried out a series of tests in order to determine the required current density for the electrochemical release. Figure 10 shows the results of these tests in terms of current density (5–350 mA/cm²) vs. the release time for 3000 Å gold membranes having 0.02 mm² of exposed area. At a current density of 35 mA/cm², the exposed areas are completely removed in 30 sec with the final release completed in 1–2 min (i.e., 5–10 μm undercut which is critical for the valve release process). Bubble generation due to electrolysis was observed at current densities larger than 35 mA/cm². These bubbles prevent the undercut process by masking the unexposed gold areas. Figure 11 shows photographs of a micromachined

Fig. 11 Photographs of the valve (left) before and (right) after release

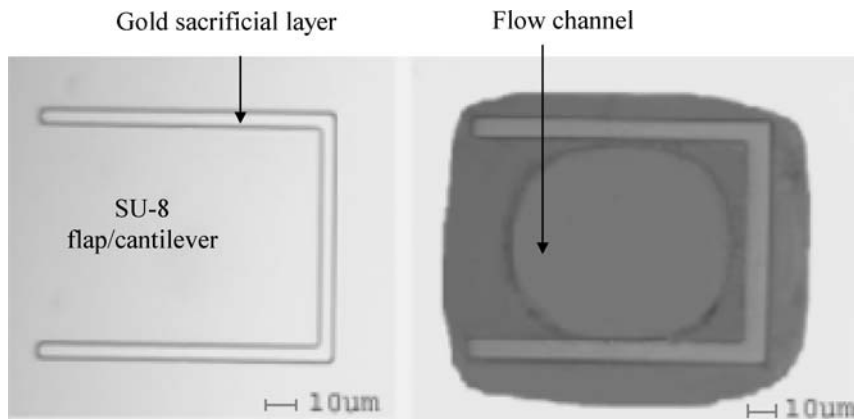
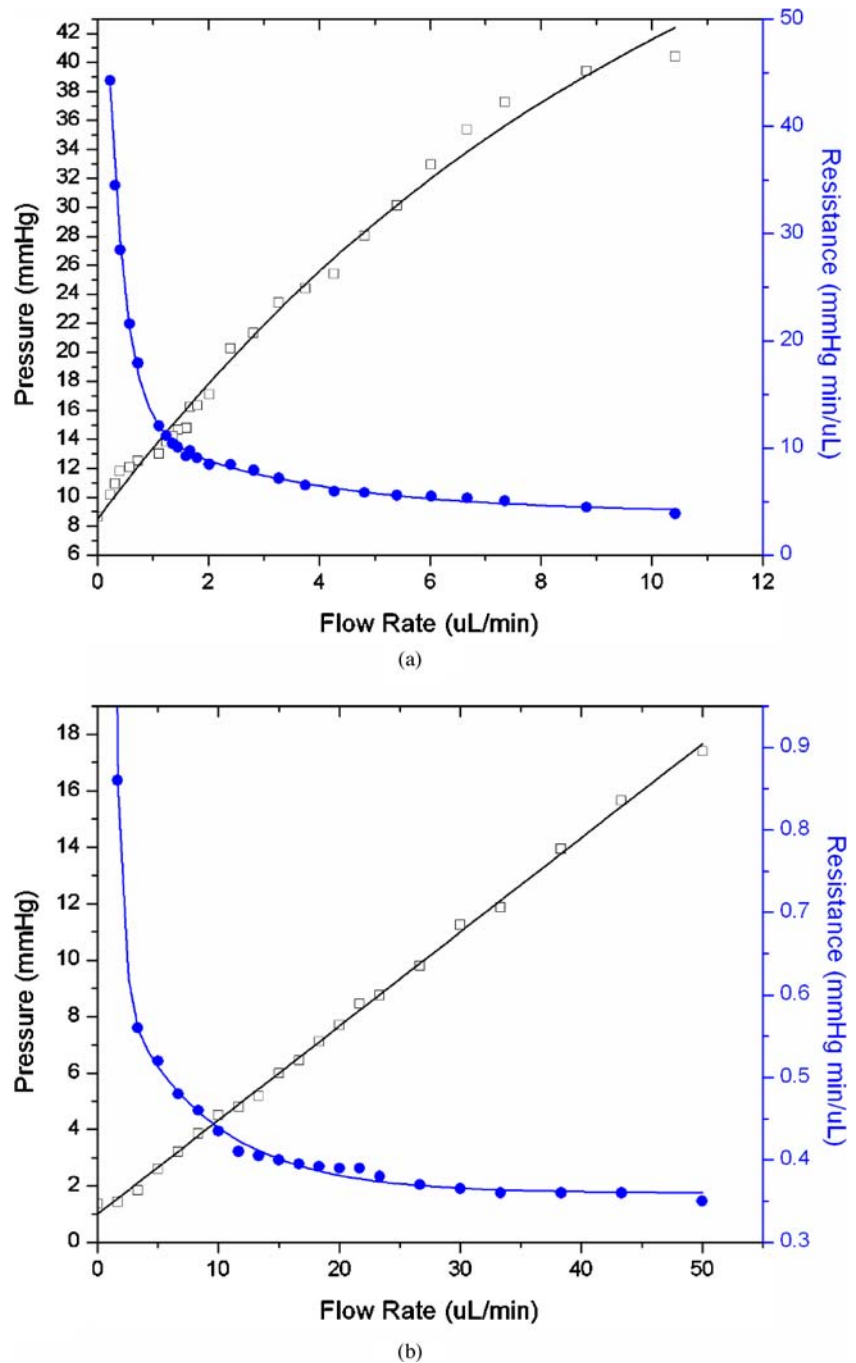


Fig. 12 The measurement results of the pressure head (left) and flow resistance (right) vs. flow rate of microvalves of (a) $50 \times 50 \mu\text{m}^2$ flow channel and (b) $100 \times 100 \mu\text{m}^2$ flow channel

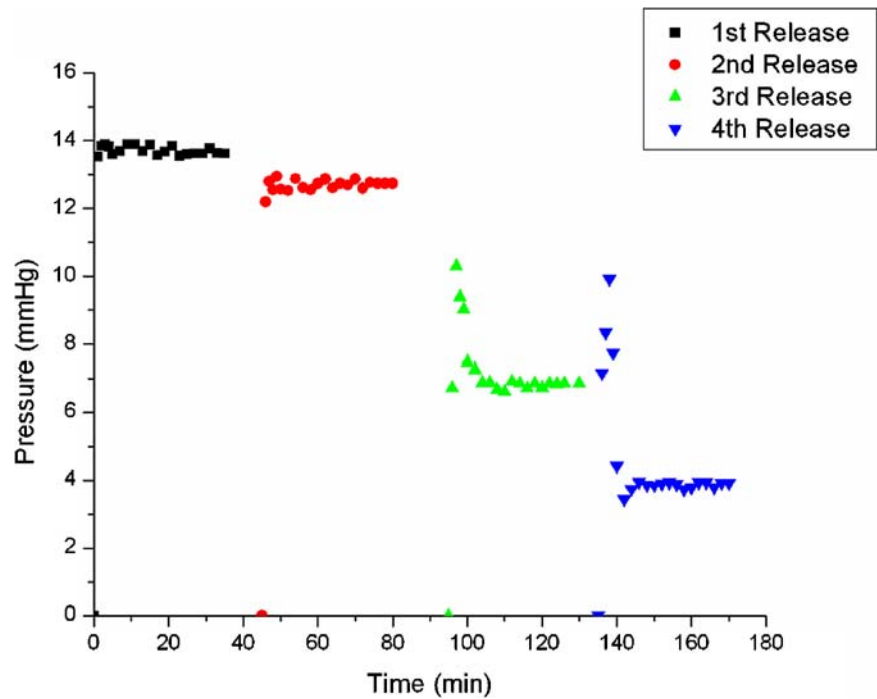


check-valve before and after the electrochemical release by applying a current density of 35 mA/cm^2 for 1 min. We also performed bending test to study the flexibility and reliability of the SU-8 flaps. For a $5 \mu\text{m}$ -thick $100 \mu\text{m}$ -long SU-8 flap, 45 degree bending test is conducted by applying a force through a probe. After 100 cycles of bending, no apparent deformation is observed.

Figure 12 shows the flow measurement results (pressure and flow resistance vs. flow rate) of two individual check-

valves, one flow channel is $50 \times 50 \mu\text{m}^2$ and the other is $100 \times 100 \mu\text{m}^2$ from the gravity characterization test. It indicates a nonlinear flow behavior of a decreasing flow resistance with closing pressures of 8.8 and 1.4 mmHg. As expected, the valve exhibits nonlinear fluidic behavior due to the pressure response of the cantilever beam structure, i.e., the higher the pressure, the larger the displacement of valve flap, and therefore the much larger the flow rate and smaller the flow resistance. Figure 13 shows the pressure

Fig. 13 The pressure measurement results for the check-valve characteristic tests illustrating the basic forward operation of the device



measurement results for syringe-pump driven constant flow tests of 4 microvalves released consecutively, which are all $50 \times 50 \mu\text{m}^2$ flow channel design, at a physiologically related flow rate of $10 \mu\text{L}/\text{min}$. The multi-stage fluidic performance has been demonstrated clearly.

4.2 Variable length cantilever microvalve

For these microvalves, similar to the previous results, a current density of $35 \text{ mA}/\text{cm}^2$ resulted in the release of

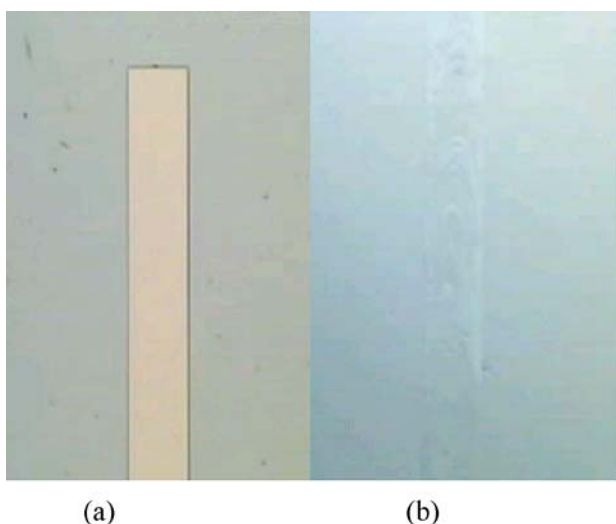


Fig. 14 Microscopic photographs of a gold strip in the variable length cantilever valve (a) before and (b) after electrochemical release

gold anchors in 2 min and gold strips in 10 min. Figure 14 shows microscopic photographs of the valve gold strip before and after release. Figure 15 shows the measurement results of the pressure head (left) and flow resistance (right) vs. flow rate of a microvalve with the cantilever flap having a width of 1.5 mm and a length of 4 mm. As expected, the valve exhibits nonlinear fluidic behavior due to the pressure response of the cantilever beam structure, i.e., the higher the pressure, the larger the displacement of valve flap, and therefore the much larger the flow rate and smaller the flow resistance. Figure 15 also indicates a closing pressure of 7.2 mmHg. Following the dissolution of each anchor, deionized (DI) water at $10 \mu\text{L}/\text{min}$ flow rate is injected into the microvalve. Figure 16 shows the pressure measurement results for the check-valve illustrating the basic forward operation of the device. Opening pressures of 178, 78, 26, 12 mmHg and stabilized pressure of 145, 72, 22, 7 mmHg show four-stage performance by releasing the gold strips sequentially.

5 Conclusions

In this paper, we report on two designs of remotely adjustable check-valves for implantable biomedical microsystems, based on an electrochemical release mechanism. Release tests with a telemetrically powered current source indicated an optimum current density of $35 \text{ mA}/\text{cm}^2$. Both gravity and syringe-pump driven flow are used to characterize the valve

Fig. 15 The measurement results of the pressure head (left) and flow resistance (right) vs. flow rate of a microvalve with the cantilever flap having a width of 1.5 mm and a length of 4 mm

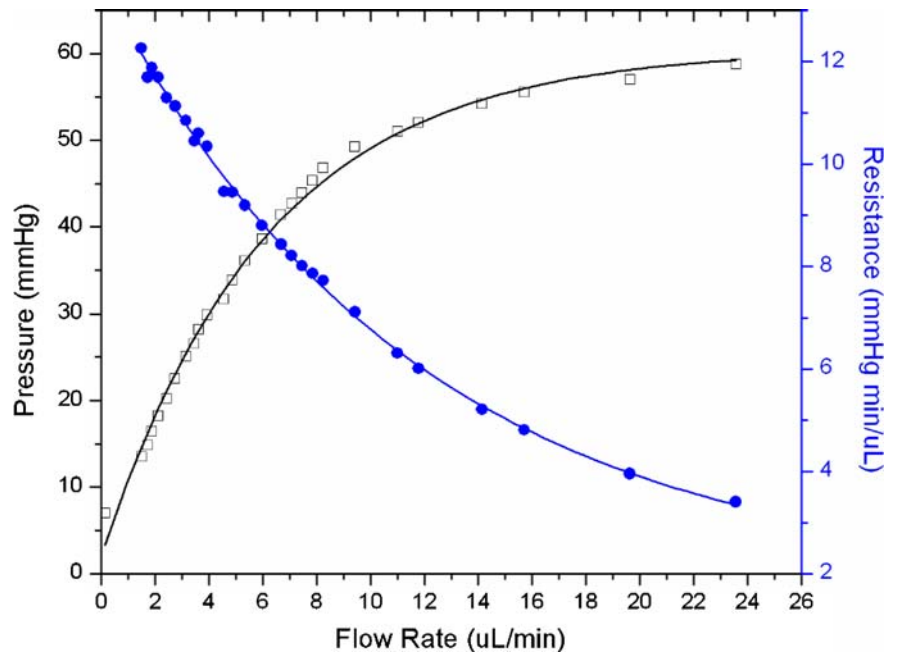
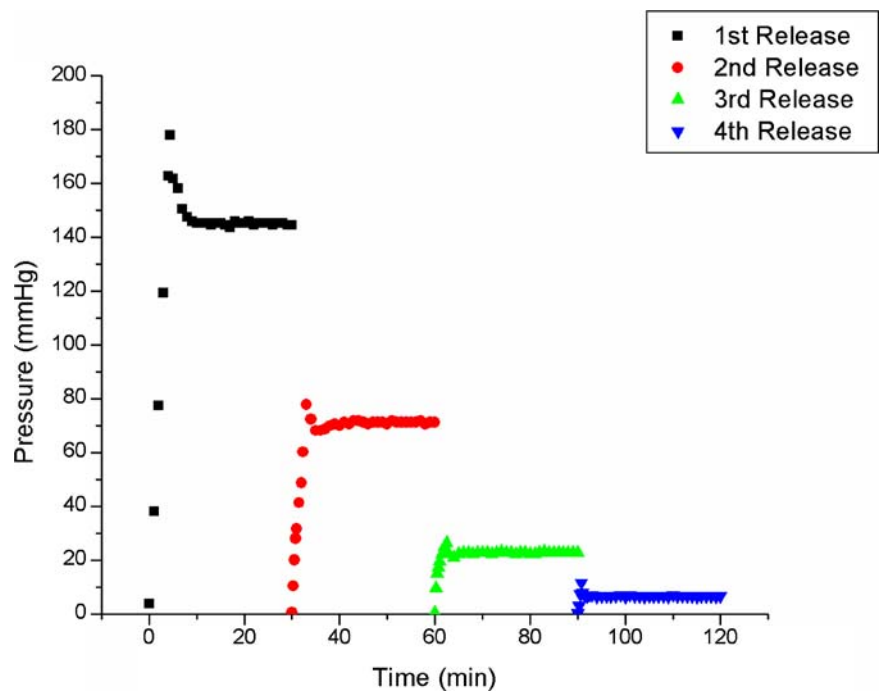


Fig. 16 The pressure measurement results for the check-valve characteristic tests illustrating the basic forward operation of the device



performance. The multi-stage fluidic performance (e.g. flow resistance and opening pressure) has been demonstrated clearly.

Acknowledgments The authors would like to thank Drs. Jay McLaren and Douglas Johnson of the Mayo Clinic and Foundation for valuable discussions. We also would like to thank Prof. David Brown of the Ophthalmology Department of the University of Minnesota for valuable advice. This work was supported by the NSF CAREER award BES-0093604 to Dr. Babak Ziaie.

References

J.D. Brown and R.F. Brubaker, *Ophthalmology* **96**, 1468–1470 (1989).
 D.T. Gretzinger, J.A. Cafazzo, J. Ratner, A.C. Easty, and J.M. Conly, *Proceedings of the IEEE EMBS* **95**, 673–674 (1995).
 L. Guerin, M. Bossel, M. Demierre, S. Calmes, and P. Renaud, *Proceedings of the IEEE Transducers* **97**, 1419–1422 (1997).

- N. LaBianca and J. Delorme, Proceedings of the SPIE **2438**, 846–852 (1995).
- H. Lorenz, M. Despont, M. Fahmi, N. LaBianca, P. Vettiger, and P. Renaud, Journal of Micromechanics and Microengineering **7**, 121–124 (1997).
- H. Lorenz, M. Laudon, and P. Renaud, Microelectronic Engineering **41–42**, 371–374 (1998).
- L. Low, S. Seetharaman, K. He, and M.J. Madou, Sensors and Actuators B: Chemical **67**, 149–160 (2000).
- T. Pan, J.D. Brown, and B. Ziaie, Proceedings of the IEEE EMBS **2**, 1830–1833 (2002).
- T. Pan, Z. Li, J.D. Brown, and B. Ziaie, Proceedings of the IEEE EMBS **3**, (2003).
- T. Pan, M.S. Stay, V.H. Barocas, J.D. Brown, and B. Ziaie, IEEE Transactions on Biomedical Engineering **52**, 948–951 (2005).
- J.M. Porter, C.H. Krawczyk, and R.F. Carey, Ophthalmology **104**, 1701–1707 (1997).
- Y. Qing, J.M. Bauer, J.S. Moore, and D.J. Beebe, Applied Physics Letters **78**, 2589–2591 (2001).
- J. Santini, M. Cima, and R. Langer, Nature **397**, 335–338 (1999).
- J. Santini, A. Richards, R. Scheidt, M. Cima, and R. Angewandte, Chemie **39**, 2396–2407 (2000).
- M.B. Shields, *Textbook of Glaucoma*, 5th ed. (Philadelphia, Williams and Wilkins, 1998).
- C.H. Tsau, S.M. Spearing, and M.A. Schmidt, Journal of Microelectromechanical Systems **11**(6), 641–647 (2002).
- X.Q. Wang, Q. Lin, and Y.C. Tai, Proceedings of the IEEE MEMS **99**, 177–182 (1999).
- H.J. Yoon, J.M. Jung, J.S. Jeong, and S.S. Yang, Sensors and Actuators A: Physical **110**, 68–76 (2004).